A Modified Top-of-the-Barrier Model for Graphene and Its Application to Predict RF Linearity

Ahsan U. Alam[1], Kyle D. Holland[1], Sabbir Ahmed[1], Diego Kienle[2], and Mani Vaidyanathan[1]
[1]Department of Electrical and Computer Engineering, University of Alberta, Edmonton, AB T6G 2V4, Canada
[2]Theoretische Physik I, Universität Bayreuth, Bayreuth, Germany
E-mail: maniv@ualberta.ca

***Abstract*—We develop a modified top-of-the-barrier model (TBM) for simulating graphene FETs. Our model captures band-to-band (Klein-Zener) tunneling, which is important in zero-bandgap materials, and it accounts for variations in the densities of states between the channel and the source and drain regions. The model is benchmarked against a sophisticated self-consistent NEGF solver and shows very good quantitative agreement. The utility of our modified TBM is demonstrated by investigating and comparing the RF linearity of graphene FETs to that of CNFETs and conventional MOSFETs.**

Keywords—band-to-band tunneling, density of states, field-effect transistor, graphene, linearity, top-of-the-barrier model.

I. Introduction

The excellent electronic properties of graphene are believed to make it a promising alternative to silicon for use in future electronics, particularly for analog circuit applications. As the down-scaling of graphene channels continues, compact modeling approaches that can tractably predict the terminal behavior, including effects arising from the zero bandgap --- such as variations in the densities of states between the channel and source and drain regions [1] and band-to-band tunneling [2] --- will be essential to explore graphene's circuit capabilities.

To date, the amount of work done on modeling graphene field-effect transistors (GFETs) has been significant. The reported approaches range from semi-classical, top-of-the-barrier models (TBMs) [3, 4] to numerically involved quantum-mechanical solvers based on non-equilibrium Green's functions (NEGF) [5-8]. The quantum-mechanical solvers, although complex and numerically demanding, are necessary to provide rigorous theoretical benchmarks, while semi-classical TBMs can provide reasonably accurate results when speed and simplicity matter, such as for compact models.

In this work, we present a way to simulate electronic transport in GFETs through a *modified* TBM [9] that captures both variations in the densities of states and band-to-band tunneling, while remaining numerically efficient. The new model is shown to produce accurate results when compared to a more rigorous, self-consistent, quantum-transport solver based on NEGF [5], and its potential is demonstrated by investigating the radio-frequency (RF) linearity of GFETs. RF linearity is an important transistor property that is relevant for a variety of circuit applications, but which is notoriously difficult to predict, requiring both accuracy and tractability in the modeling approach.

II. Theory

As graphene devices mature beyond the research stage, doped MOSFET-style devices will be necessary to obtain better performance than the Schottky-barrier devices prevalent today [10, 11]. Based on this observation, and as a starting point, we assume the device geometry shown in Fig. 1(a), consisting of an intrinsic channel region surrounded by heavily doped source and drain regions. For reference throughout this discussion, a plot of the Dirac-point energy E_{DP} versus position x under typical operating conditions in such a device is shown in Fig. 1(b).

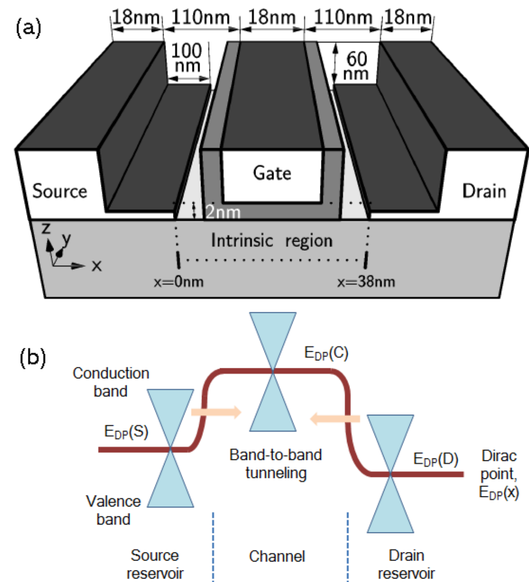

Fig. 1. (a) Device geometry of the simulated GFET [5]. (b) Dirac-point energy $E_{\mathrm{DP}}(x)$ versus position x, where the superimposed cones represent graphene's band structure.

Top-of-the-barrier approaches [9] have been widely used to model ballistic transport in field-effect transistors. Despite its simplicity, the conventional TBM has been shown to offer good accuracy when compared to more rigorous simulation methodologies for CNFETs and MOSFETs [9, 12]. The most striking difference between the channel materials used in such FETs and graphene is that the bandgap is zero in graphene. The zero bandgap causes the transport to be strongly ambipolar, *i.e.*, both electrons and holes contribute to the charge flow. This ambipolar character of graphene can be taken into account by modifying the transport equations of the conventional TBM [9] in the following manner:

$$n_{\mathrm{S/D}} = \frac{1}{2}\int_{E_{\mathrm{DP}}(C)}^{\infty} D_C(E) f(E - E_{\mathrm{F,S/D}})\mathrm{d}E \quad (1)$$

$$p_{\mathrm{S/D}} = \frac{1}{2}\int_{-\infty}^{E_{\mathrm{DP}}(C)} D_C(E)[1 - f(E - E_{\mathrm{F,S/D}})]\mathrm{d}E \quad (2)$$

$$Q = q(p_S + p_D) - q(n_S + n_D) \quad (3)$$

$$I_{\mathrm{S/D}} = q v_F (p_{\mathrm{S/D}} - n_{\mathrm{S/D}}) \quad (4)$$

$$I_{\mathrm{DS}} = I_D - I_S \quad (5)$$

where $n_{\mathrm{S/D}}$ and $p_{\mathrm{S/D}}$ are the electron and hole density of the channel arising from contributions from the source/drain (S/D), respectively; $E_{\mathrm{DP}}(C)$ is the channel Dirac-point energy, determined by shifting its equilibrium position $E_{\mathrm{DP,E}}(C)$ by the self-consistent potential U_{SCF}, *i.e.*, $E_{\mathrm{DP}}(C) \equiv E_{\mathrm{DP,E}}(C) - U_{\mathrm{SCF}}$; $D_C(E)$ is the channel density of states (DOS); $f(E)$ is the Fermi-Dirac distribution function; $E_{\mathrm{F,S/D}}$ is the chemical potential of the source/drain reservoir; Q is the total charge in the channel, which is used in Poisson's equation to determine U_{SCF}; $I_{\mathrm{S/D}}$ is the conventional current from the source/drain; and I_{DS} is the net drain-to-source current.

Although the TBM specified by (1)-(5) can capture the ambipolar nature of transport in graphene, it still misses important physics. First, the lack of a bandgap in graphene results in significant band-to-band tunneling, a quantum-mechanical effect that the conventional TBM does not include. Second, the conventional TBM cannot model the difference in the DOS between the doped reservoirs and the channel. These limitations can be overcome by amending the TBM through the following steps. First, band-to-band tunneling is introduced to the TBM with the WKB approximation [2]. Second, we construct an "effective DOS" that accounts for the fact that the densities of states in the source and drain reservoirs vanish at the local Dirac points [$E_{\mathrm{DP}}(S)$ and $E_{\mathrm{DP}}(D)$ in Fig. 1(b)], preventing any transmission at these energies [5].

A. Effective Density of States

The effect on transport due to the lack of states at the Dirac points in the source and drain reservoirs can be included in the top-of-the-barrier formalism by replacing the *channel* density of states $D_C(E)$ with two *effective* densities of states. Our refined model hence replaces $D_C(E)$ with $D_{\mathrm{SC}}(E)$ for transport from the source to the channel and $D_{\mathrm{DC}}(E)$ for transport from the drain to the channel. At each energy, the effective DOS functions contain the minimum density of states existing between the corresponding reservoir (source or drain) and the channel. Equations (1) and (2) can therefore be re-written as

$$n_{\mathrm{S/D}} = \frac{1}{2}\int_{E_{\mathrm{DP}}(C)}^{\infty} D_{\mathrm{SC/DC}}(E) f(E - E_{\mathrm{F,S/D}})\mathrm{d}E \quad (6)$$

$$p_{\mathrm{S/D}} = \frac{1}{2}\int_{-\infty}^{E_{\mathrm{DP}}(C)} D_{\mathrm{SC/DC}}(E)[1 - f(E - E_{\mathrm{F,S/D}})]\mathrm{d}E \quad (7)$$

It is worth mentioning here that in the conventional TBM [9], the doped source and drain are assumed to be *infinite* reservoirs, in which case the "effective DOS" $D_{\mathrm{SC/DC}}(E)$ always reduces to the channel DOS $D_C(E)$, as it is the channel that determines (limits) the available states for transport at all energies.

Fig. 2(a) shows the effective DOS $D_{\mathrm{SC}}(E)$, which is zero at the Dirac-point energies associated with the source and the channel, and Fig. 2(b) shows the corresponding Landauer transmission function for the electron/hole transport, which is proportional to $D_{\mathrm{SC}}(E)$ for the energies shown; as illustrated, the transmission vanishes at those energies where $D_{\mathrm{SC}}(E)$ vanishes, in agreement with results obtained from the quantum-mechanical NEGF solver reported in [5]. For reference, the DOS and the transmission function from the *conventional* TBM are also plotted (dash-dot).

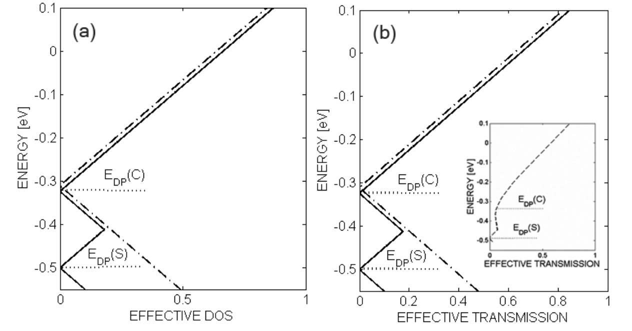

Fig. 2. (a) Effective (normalized) source-to-channel DOS $D_{\mathrm{SC}}(E)$ of the *modified* TBM, being zero at the indicated Dirac-point energies, and (b) respective effective (normalized) transmission function describing the source-to-channel transport. (Inset: transmission obtained from a NEGF solver under similar operating conditions [5].) The DOS and the transmission function for the *conventional* TBM are also plotted (dash-dot) for comparison.

B. Band-to-Band Tunneling

Graphene is a zero-bandgap semiconductor. This unique property makes it considerably different from its competitors, such as silicon and carbon nanotubes. The lack of a bandgap means that the valence band in the channel actively participates in transport along with the conduction band. For example, under certain gate biases, the carriers in the conduction band in the doped source and drain reservoirs can tunnel through the potential barrier at the corresponding reservoir-to-channel interface and enter the channel valence band [Fig. 1(b)]. This additional transport path, *i.e.*, in addition to regular thermionic transport over the barrier, must be taken into account in graphene to predict the terminal behavior.

In order to properly model the band-to-band tunneling in a graphene FET, we have modified the conventional TBM equations by introducing a tunneling probability $T_{\mathrm{KZ,S/D}}(E)$ as a function of energy E, so that (6) and (7) become

$$n_{\mathrm{S/D}} = \frac{1}{2}\int_{E_{\mathrm{DP}}(C)}^{\infty} T_{\mathrm{KZ,S/D}}(E) D_{\mathrm{SC/DC}}(E) f(E - E_{\mathrm{F,S/D}})\mathrm{d}E \quad (8)$$

$$p_{\mathrm{S/D}} = \frac{1}{2}\int_{-\infty}^{E_{\mathrm{DP}}(C)} T_{\mathrm{KZ,S/D}}(E) D_{\mathrm{SC/DC}}(E)\left[1 - f\left(E - E_{\mathrm{F,S/D}}\right)\right]\mathrm{d}E \quad (9)$$

where $T_{\mathrm{KZ,S/D}}(E)$ is the band-to-band (Klein-Zener) tunneling probability from the source/drain reservoir to channel. The

Klein-Zener tunneling probability, unlike conventional quantum tunneling, can assume a value of unity when a carrier encounters a potential barrier, depending on its direction of travel, and within the WKB approximation, this tunneling probability $T_{\mathrm{KZ,S/D}}(k_\perp)$ can be expressed as a function of the longitudinal component of the wave vector $k_\perp$ [2]:

$$T_{\mathrm{KZ,S/D}}(k_\perp) = \exp\left(-\pi {k_\perp}^2 \hbar v_F / q\varepsilon_{\mathrm{S/D}}\right) \quad (10)$$

where v_F is the Fermi velocity in graphene (~10^5 m/s), q is magnitude of the electronic charge, and $\varepsilon_{\mathrm{S/D}}$ is the electric field of the potential barrier at the source/drain reservoir-to-channel interface, given by $\varepsilon_{\mathrm{S/D}} = V_{\mathrm{diff,S/D}}/\Delta x$, with $V_{\mathrm{diff,S/D}}$ being the voltage across the source/drain barrier and Δx being an effective width. By a change of variables, the tunneling probability can be rewritten as a function of energy:

$$T_{\mathrm{KZ,S/D}}(E) = \exp\left(-a/2\right) J_0(a/2) \quad (11)$$

where J_0 is the zeroth order Bessel function of the first kind and $a = \pi E^2 / q\hbar^2 v_F \varepsilon_{\mathrm{S/D}}$.

These amendments lead to a modified set of TBM equations by which we are able to quantitatively match a GFET's behavior as predicted by more rigorous NEGF simulations [5], including the transistor's current-voltage curves, unity current-gain frequency f_T, transconductance g_m, and output conductance g_d. The usual fitting parameters [9] accompanied with the TBM, *i.e.*, α_g, α_d, and α_s, along with the new fit parameter Δx, are used to calibrate our model. The resulting solver is then used to determine the RF linearity of graphene using the method described in [12].

III. Results and Discussion

Our modeled GFET [Fig. 1(a)] has dimensions identical to the device investigated in [5], including a gate length of 18 nm. As a first step, the three fitting parameters α_g, α_d, and α_s were used to fit the TBM output with the NEGF data following the procedure of [9]. The fourth fitting parameter Δx was then introduced (accompanied by a tweaking of the initial values of α_g, α_d, and α_s) to further enhance the match. For the modeled GFET, we obtained $\alpha_g = 0.76$, $\alpha_d = 0.17$, $\alpha_s = 0.07$, and $\Delta x = 0.43$ nm.

Of particular note is the magnitude of α_d obtained during the fitting. The value in the conventional TBM is 0.033, a value much smaller than the value of 0.17 observed with our modified approach. The new value is consistent with results from [5], which predict a more dominant drain capacitance than is normally observed. The modified TBM thus more closely matches the underlying physics observed in much more detailed calculations, while still running in a fraction of the time.

It should also be noted that during fitting of both the conventional TBM and the modified TBM with NEGF data, an effective oxide thickness of 1.5 nm was needed for proper matching. This value differs from the actual value of 2 nm [indicated in Fig. 1(a)] to account for fringe capacitance in the real structure, which is automatically included in the NEGF but which is excluded in the TBM.

Fig. 3 shows the current-voltage characteristics of the GFET from our modified TBM solver and the self-consistent NEGF solver [5]. Considering the simplicity of our modified TBM, the agreement is quite remarkable. Fig. 4 demonstrates that the developed model not only matches the $i_D - v_G$ output characteristics, but also is in good agreement with more sensitive quantities involving derivatives, such as the transconductance g_m and output conductance g_d; in addition, our modified TBM shows a clear improvement towards the NEGF solution over the conventional TBM, particularly at lower v_G, where the magnitude of the tunneling current through the barrier is significant. Finally, we have plotted the second derivatives of the current in Fig. 5, which shows an even better improvement over the conventional model. Such improved agreement is important for an accurate prediction of the device's properties for analog circuit applications, such as RF linearity, which requires a proper modeling of the slope and curvature of the transistor characteristics versus voltage.

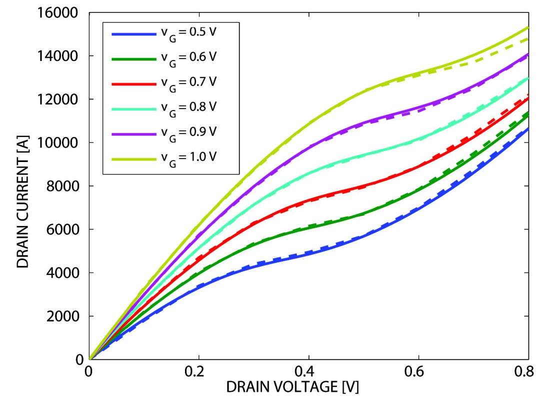

Fig. 3. Current-voltage characteristics of the graphene field-effect transistor from NEGF (dash) and the modified top-of-the-barrier solver (solid).

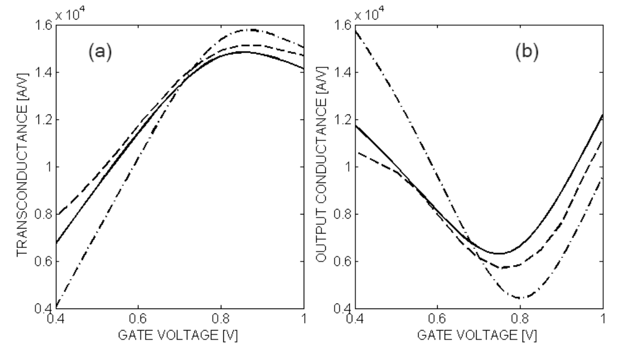

Fig. 4. (a) Transconductance and (b) output conductance versus gate voltage of the graphene field-effect transistor from NEGF (dash), conventional top-of-the-barrier model (dash-dot), and modified top-of-the-barrier model (solid).

We used our modified TBM solver to determine the element values of a nonlinear, small-signal equivalent circuit (Fig. 6) for the GFET of Fig. 1(a), following the approach described in [12]. Here, C_{ge}, C_{se}, and C_{de} are the electrostatic capacitances of the GFET, which we assume to be linear as a first approximation, as discussed in [12]; C_{sq} and C_{dq} are the nonlinear source and drain quantum capacitances, respectively; and i_{ts} and i_{td} are the nonlinear current sources that model the

quasi-static transport currents of the device. It is worth noting that due to the higher-order derivatives involved, accurately predicting these nonlinear elements requires the use of our modified TBM; use of the conventional TBM leads to significant differences compared to the benchmark NEGF data, as illustrated by the results in Figs. 4 and 5.

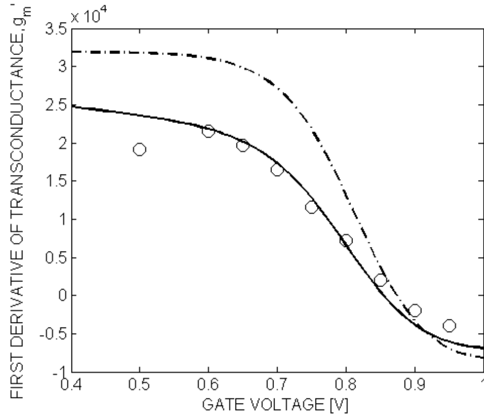

Fig. 5. First derivative of transconductance with respect to gate voltage of the graphene field-effect transistor plotted versus gate voltage. Shown are results from the conventional top-of-the-barrier model (dash-dot) and modified top-of-the-barrier model (solid). The modified TBM shows excellent agreement with NEGF data (open circles).

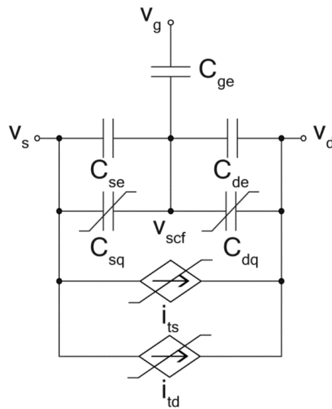

Fig. 6. Nonlinear small-signal equivalent circuit of a ballistic GFET.

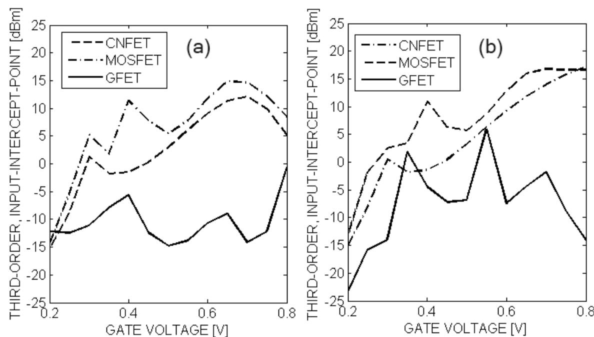

Fig. 7. IIP3 versus gate voltage, *with the drain voltage held fixed at (a) 0.5 V and (b) 0.8V*, of the graphene FET compared to its CNFET and MOSFET counterparts.

Once the circuit is formed, the harmonic balance solver in Microwave Office [13] can be used to determine the GFET's third-order, input-intercept point (IIP3). Fig. 7 (a) shows that for a drain voltage of 0.5 V, the IIP3 of the GFET is significantly worse than its CNFET and MOSFET counterparts, where the latter have dimensions and an oxide capacitance identical to the GFET. However, by increasing the drain voltage to 0.8 V, the linearity can be improved and becomes closer to that of CNFETs and MOSFETs, as shown in Fig. 7 (b). Unlike a CNFET and a MOSFET, where the drain biasing has a negligible effect on the IIP3, our results show that the linearity of GFETs is quite sensitive to the drain bias. Further such insights into the linearity and RF behavior of graphene-based devices can be obtained by exploiting our modified top-of-the-barrier model, and these will be reported elsewhere.

IV. CONCLUSIONS

We developed a modified top-of-the-barrier model for graphene field-effect transistors that includes variations in the reservoir versus channel densities of states and band-to-band tunneling. The model shows excellent agreement with state-of-the-art, quantum-mechanical approaches based on NEGF and allows for the development of accurate, practical circuit models. The utility of the new model is demonstrated by exploring the RF linearity of graphene transistors.

ACKNOWLEDGMENT

The authors are thankful to AWR Corporation, El Segundo, CA, for providing Microwave Office and technical support.

REFERENCE

[1] S. Datta, *Quantum Transport: Atom to Transistor.* Cambridge University Press, New York, 2005.

[2] N. Vandecasteele *et al.*, "Current-voltage characteristics of graphene devices: interplay between Zener-Klein tunneling and defects," *Physical Review B,* vol. 82, pp. 045416-25, 2010.

[3] G. Liang *et al.*, "Performance projections for ballistic graphene nanoribbon field-effect transistors," *IEEE Trans. Electron Devices,* vol. 54, pp. 677-82, 2007.

[4] S. O. Koswatta *et al.*, "Ultimate RF performance potential of carbon electronics," *IEEE Trans. Microwave Theory Tech.,* vol. 59, pp. 2739-50, 2011.

[5] K. D. Holland *et al.*, "RF performance limits and operating physics arising from the lack of a bandgap in graphene transistors," *IEEE Transactions on Nanotechnology,* Accepted for Publication, 2013.

[6] G. Liang *et al.*, "Ballistic graphene nanoribbon metal-oxide-semiconductor field-effect transistors: a full real-space quantum transport simulation," *J. Appl. Phys.,* vol. 102, pp. 054307- 1-7, 2007.

[7] G. Fiori and G. Iannaccone, "Simulation of graphene nanoribbon field-effect transistors," *IEEE Electron Device Lett.,* vol. 28, pp. 760-2, 2007.

[8] T. Low *et al.*, "Conductance asymmetry of graphene p-n junction," *IEEE Trans. Electron Devices,* vol. 56, pp. 1292-9, 2009.

[9] A. Rahman *et al.*, "Theory of ballistic nanotransistors," *IEEE Trans. Electron Devices,* vol. 50, pp. 1853-64, 2003.

[10] K. Alam, "Transport and performance of a zero-Schottky barrier and doped contacts graphene nanoribbon transistors," *Semiconductor Science and Technology,* vol. 24, pp. 015007-14, 2009.

[11] Y. Yoon *et al.*, "Performance comparison of graphene nanoribbon FETs with Schottky contacts and doped reservoirs," *IEEE Trans. Electron Devices,* vol. 55, pp. 2314-23, 2008.

[12] A. U. Alam *et al.*, "RF linearity potential of carbon-nanotube transistors versus MOSFETs," *IEEE Transactions on Nanotechnology,* vol. 12, pp. 340-51, 2013.

[13] AWR Corporation, "Microwave Office," vol. 10.04.6079.1, 2013.